Green Chemistry

PAPER

View Article Online
View Journal

Cite this: DOI: 10.1039/d0gc03828h

Enhancing the multi-functional properties of renewable lignin carbon fibers *via* defining the structure–property relationship using different biomass feedstocks†

Qiang Li, [a,b] Cheng Hu,[a,b] Mengjie Li,[a,b] Phuc Truong,[c] Jinghao Li,[a,b] Hao-Sheng Lin,[a,d] Mandar T. Naik,[e] Sisi Xiang, [f] Brian E. Jackson,[g] Winson Kuo, [f] Wenhao Wu,[h] Yunqiao Pu, [i] Arthur J. Ragauskas [i,j,k] and Joshua S. Yuan *[a,b]

Lignin has been explored extensively as a renewable precursor for carbon materials, considering its abundance as a major component of plant cell walls and its sustainability as a byproduct of both lignocellulosic biorefinery and the paper-making industry. Despite the extensive efforts to define the process–property relationship, it remains largely unknown how lignin biosynthesis and its chemistry would impact the resultant carbon fiber properties, for both mechanical and electroconductive performances. Such inadequate understanding fundamentally limits feedstock design and selection to improve carbon fiber properties toward broader commercial applications. Using lignin from a broad range of biomass feedstocks for carbon fiber manufacturing, we have fundamentally explored the structure–function relationship between lignin chemistry and carbon fiber performance. Specifically, lignin extracted from hardwood (sugar maple), softwood (loblolly pine and red cedar), and herbaceous plants (corn stover and switchgrass) was used for carbon fiber manufacturing, considering the very different lignin structures from these feedstocks. Linear regression models were established to define the relationship between carbon fiber mechanical properties and lignin structural characteristics. The results highlighted that the content of *β*-*O*-4 linkages correlates significantly with the tensile strength and elastic modulus of lignin carbon fibers, indicating that more linear *β*-*O*-4 linkages would promote the carbon fiber mechanical performance. Moreover, electroconductive properties are essential for broader energy device application of lignin-based carbon fibers, yet the mechanisms controlling their electroconductivity are largely unknown. We hereby demonstrated that a higher *β*-*O*-4 content also promotes the electroconductivity of lignin carbon fibers. Microstructure analysis further revealed that the crystallite size and content of the pre-graphitic turbostratic carbon structure in lignin-based carbon fibers were enhanced as the *β*-*O*-4 linkages increased. The content of *β*-*O*-4 linkages has shown a strong correlation with the crystallite content in a linear regression model. This study thus revealed the underlying mechanisms regarding how the lignin structure *in planta* defines the resultant carbon fiber properties. Moreover, the study also highlighted the correlation between the mechanical and electroconductive properties of lignin-based carbon fibers, both of which were defined by the lignin structure.

Received 12th November 2020,
Accepted 24th February 2021

DOI: 10.1039/d0gc03828h

rsc.li/greenchem

[a]*Synthetic and Systems Biology Innovation Hub, Department of Plant Pathology and Microbiology, Texas A&M University, College Station, TX 77843, USA. E-mail: syuan@tamu.edu*
[b]*Department of Chemical Engineering, Texas A&M University, College Station, TX 77843, USA*
[c]*Soft Matter Facility, Texas A&M University, College Station, TX 77843, USA*
[d]*Department of Soil and Crop Science, Texas A&M University, College Station, TX 77843, USA*
[e]*Department of Molecular Pharmacology, Physiology and Biotechnology, Brown University, Providence, RI 02903, USA*
[f]*Materials Characterization Facility, Texas A&M University, College Station, TX 77843, USA*
[g]*Department of Horticultural Science, North Carolina State University, Raleigh, NC 27695, USA*
[h]*Department of Physics and Astronomy, Texas A&M University, College Station, TX 77843, USA*
[i]*Joint Institute for Biological Sciences, Biosciences Division, Oak Ridge National Laboratory, Oak Ridge, TN 37831, USA*
[j]*Department of Chemical and Biomolecular Engineering, The University of Tennessee, Knoxville, TN 37996-2200, USA*
[k]*Department of Forestry, Wildlife and Fisheries, Center for Renewable Carbon, Institute of Agriculture, The University of Tennessee, Knoxville, TN 37996-2200, USA*

†Electronic supplementary information (ESI) available. See DOI: 10.1039/d0gc03828h

1. Introduction

Lignin can be considered as the second most abundant biopolymer on the Earth and is a major byproduct in pulping and biorefining industries. Among the different renewable products derived from lignin, lignin-based carbon materials have a significant and profound impact on energy and the environment. On one hand, as an abundant byproduct, the utilization of lignin as a precursor will reduce the carbon fiber cost and enable broader applications of carbon fibers in automobile, wind turbine, and aerospace industries. Such broader application of lightweight materials will improve their energy efficiency and environmental sustainability for energy and other industrial sectors.[1–6] On the other hand, the utilization of lignin for carbon fiber production will improve both the sustainability and cost-effectiveness of modern biorefining, considering the broad application, large volume, and high market value of carbon fibers.[7–9] Moreover, using a renewable precursor like lignin for carbon fiber production represents green and sustainable manufacturing for converting abundant industrial lignin waste into advanced materials. Despite the significant potential, the major challenge in the commercialization of lignin carbon fibers is their low performance as compared to the carbon fibers derived from traditional polyacrylonitrile (PAN) precursors.[8,10] The underlying mechanisms for such a low performance are still elusive, especially from the plant lignin biosynthesis and biomass feedstock perspectives.

Recent breakthroughs have focused on improving biomass processing to enhance the lignin carbon fiber performance. For example, we have previously developed novel lignin fractionation methods using enzyme mediators,[7,11,12] dialysis tubes,[7] and water[13,14] to derive lignin with more uniform molecular weights, which boosted the lignin carbon fiber mechanical performance. Despite the progress, it is still not clear how the inherent lignin structure as biosynthesized *in planta* will impact the carbon fiber performance. Biomass characteristics and lignin chemical structure are largely defined during plant cell wall thickening through several biosynthesis steps including monolignol biosynthesis, monolignol transportation outside of the plasma membrane, and lignin polymerization (lignification).[15–21] The different ratios of monolignol and the following enzymatic and non-enzymatic coupling reactions would yield lignin with diverse chemical structures. Previous research studies have focused on tailoring biomass processing to derive more processable carbohydrates,[22–28] yet very few research studies focused on how the inherent chemical structure of lignin biosynthesized *in planta* could impact the resultant material performance. We aim to address this challenge by dissecting the relationship between carbon fiber properties and biomass characteristics using feedstocks with diverse lignin structures.

In different biomass feedstocks, including herbaceous plants, softwood and hardwood, lignin biosynthesis is known to produce different monolignol proportions and chemical linkage profiles.[29] For example, ρ-coumaryl alcohol is involved in lignin biosynthesis in herbaceous plants, forming ρ-hydroxyphenyl propane-type lignin (H lignin), whilst sinapyl alcohol is the major monolignol biosynthesized in angiosperms (hardwood) for the formation of syringyl-type lignin (S lignin) (Fig. 1). Different from herbaceous plants and hardwood, gymnosperms (softwood) have guaiacyl-type lignin (G lignin) as the primary monolignol, which is biosynthesized from coniferyl alcohol (Fig. 1). Adding to the diverse monolignol structures, the three types of biomass feedstocks also contain diverse linkage profiles, where hardwood typically contains more β-*O*-4 linkages than both herbaceous plants and softwood. Herbaceous plants, softwood and hardwood have all been widely used as feedstocks for both biorefinery and pulp production.[30] In this study, we therefore focused on exploring how biomass characteristics regarding lignin structures define the microstructure and multi-functional properties of lignin carbon fibers. The new discovery will guide the feedstock development for both high-value products and fuels.

Besides mechanical properties, another largely over-looked aspect for plant-derived renewable carbon fibers is their electroconductive properties. The electroconductive properties are an important consideration for the application of lignin-based carbon fibers in energy storage applications, including as carbonaceous electrodes for lithium-ion batteries and supercapacitors.[31] Despite the extensive studies of mechanical performance, it is still largely unknown what defines the electroconductive properties of lignin-based carbon fibers and how the electroconductive performance is related to mechanical properties. Neither do we know if there is any strategy that could synergistically improve the electroconductive and mechanical properties of lignin-based carbon fibers.

In this study, we therefore elucidated the relationship between the lignin structure and multi-functional properties of carbon fibers using feedstocks with very different biomass characteristics. The carbon fiber microstructure will be investigated to reveal the underlying mechanisms for improving electroconductive and mechanical properties. The mechanistic study has guided the development of strategies to synergistically improve electroconductive and mechanical properties, as well as delivering the lignin-based carbon fibers with a comparable performance to PAN-based carbon fibers. This discovery will open up new avenues to design transformative feedstocks for both biofuels and biomaterials and to enable sustainable and cost-effective biorefining and pulping.

2. Experimental

2.1 Materials

Different biomasses of hardwood (sugar maple), softwood (red cedar and loblolly pine), and herbaceous plants (switchgrass and corn stover) were used in this research. All biomasses were milled using a Wiley miller to pass a 60-mesh screen. The milled biomasses were then extracted by benzene–ethanol extraction to remove extractives.[32] The extractive-free biomasses were stored under 4 °C until utilization.

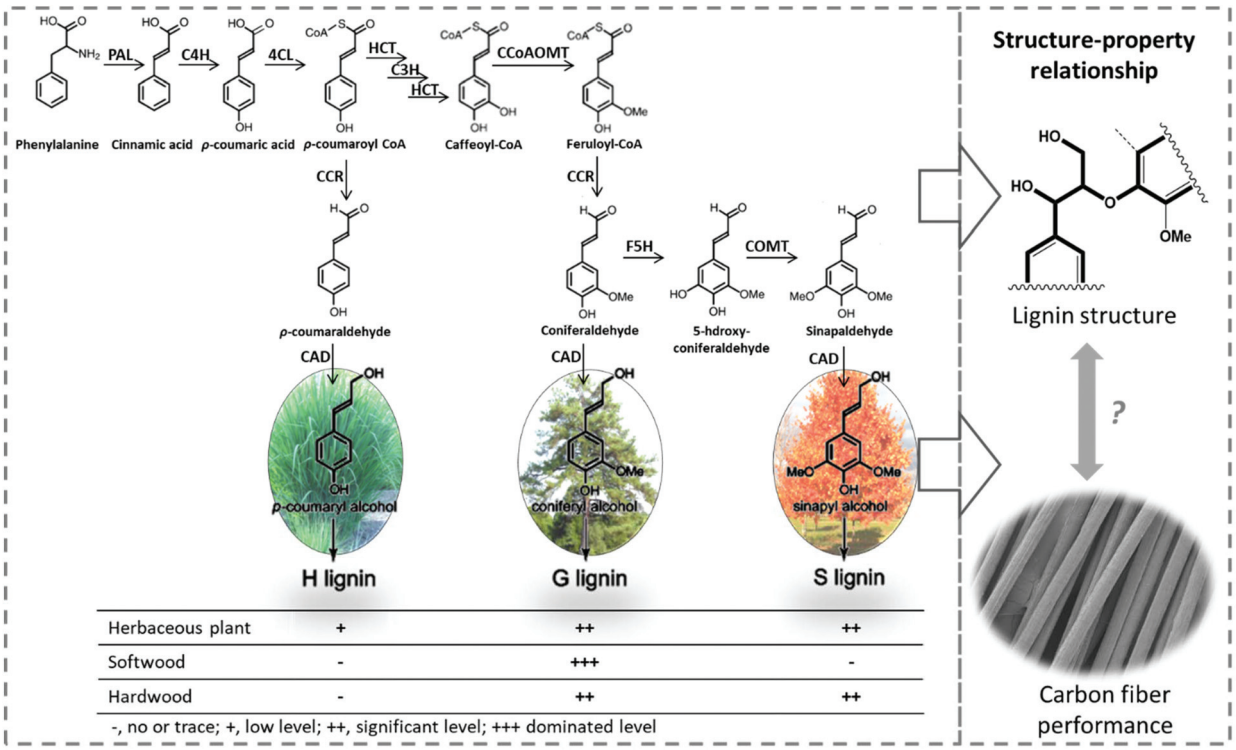

Fig. 1 The general schema of the study to use lignin from different feedstocks to reveal the structure–property relationship between the lignin chemical structure and carbon fiber performance. H, ρ-hydroxyphenyl propane; G, guaiacyl; S, syringyl.

Polyacrylonitrile (PAN) with the molecular weight (MW) of 150 000 g mol^{-1} was obtained from Pfaltz & Bauer, USA. All other chemicals used in this research were purchased from Sigma–Aldrich, USA.

2.2 Lignin preparation and characterization

Lignin extraction. Lignin was extracted by organosolv extraction using acetic acid as reported before.[33,34] Briefly, 40 g of extractive-free biomass was treated with 90% aqueous acetic acid with the addition of 0.32% sulfuric acid as the catalyst. The liquid to solid ratio was 7 : 1 for all woody samples, while this ratio was 10 : 1 for switchgrass and corn stover. The heating temperature was kept at around 118 °C in an oil bath to keep acetic acid reflux. After 3 h treatment, the pretreatment mixture was cooled down and then filtered to get a filtrate and biomass residue. The obtained filtrate was then concentrated into about 100 mL by evaporation followed by precipitation into deionized water and stirring for 30 min. After centrifugation, three times washing with deionized water, centrifugation again and lyophilization, fine powders of acetic acid lignin were obtained. The ash content of each lignin sample was measured by pyrolyzing a certain amount of lignin in a muffle furnace (575 ± 25 °C) for at least 4 h until no weight loss was measured. The very low ash content as shown in Table S2† indicated the high purity of all these lignin samples.

Fourier-transform infrared spectroscopy (FTIR). The possible carbonyl groups in the extracted lignin samples were analyzed using a Nicolet™ 380 FT-IR spectrometer equipped with an OMNI-Sampler™ ATR sampling accessory. All lignin powders were ground and dried to remove the moisture before the measurement. The spectra were recorded in the spectral range of 700–4000 cm^{-1} with a resolution of 4 cm^{-1}. For each measurement, 128 scans were collected for both the background and sample. The peak at around 1720 cm^{-1} was assigned to the carbonyl group. The FTIR spectra are as shown in Fig. S2.†

Gel permeation chromatography. The molecular weights of lignin were measured by gel permeation chromatographic (GPC) analysis after acetylation as reported before.[7] In brief, lignin samples were acetylated using acetic anhydride and pyridine (1 : 1, v/v) at room temperature overnight under magnetic stirring. After the acetylation, ethanol was added and the mixture was evaporated using a rotatory evaporator. The acetylated lignin sample was then dissolved in tetrahydrofuran (THF). A membrane filter (0.45μm) was used to filter the solution before injecting for GPC analysis on an Agilent 1200 HPLC system (Agilent Technologies, Inc., Santa Clara, CA, USA) equipped with three Waters Styragel columns (HR0.5, HR3, and HR5E; Waters Corporation, Milford, MA, USA) linked in series. An ultraviolet detector was employed for detection with wavelength setting at 270 nm. THF was used as the mobile phase and the flow rate was at 0.5 ml min^{-1}. The calibration curve was established using a series of narrow range polystyrene standards. The GPC results are presented in Table S3.†

Two-dimensional heteronuclear single quantum coherence nuclear magnetic resonance (2D HSQC NMR). Lignin interunitary linkages were characterized by 2D HSQC NMR (Bruker AVANCE 500 MHz spectrometer equipped with a cryoprobe). The extracted lignin was dissolved in 0.6 mL of DMSO-*d*6 and placed in an NMR tube. Adiabatic 2D ^{1}H–^{13}C HSQC spectra were acquired and processed with Topspin 3.2 (Bruker Biospin), as described before.[11,35] The obtained HSQC spectra were analyzed using the software MestReNova. The assignments and quantification of linkages are shown in Table S1.† For the quantification of the relative difference in the lignin linkages, the well-resolved contours of Iα, IIα, and IIIα (Fig. 7) were integrated using MestReNova software. The frequency of each linkage (Fig. 7B) was expressed as per 100 aromatic rings of the total of S, G, and H units and was calculated using the equation below:[35]

$$\text{Frequency}\,(\%) = \frac{I_x}{I_{S2/6} + I_{G2} + I_{H2/6}} \times 100\%$$

where I_x is the integration of the linkage to be calculated, which was obtained from the integrations of Iα, IIα, and IIIα, respectively. $I_{S2/6}$, I_{G2} and $I_{H2/6}$ are the integrations of the aromatic rings of $S_{2/6}$, G_2, and $H_{2/6}$ units, respectively, and a factor of 0.5 was used to adjust for S and H units. The chemical structures and NMR spectra of the $S_{2/6}$, G_2, and $H_{2/6}$ are in Fig. S1.†

2.3 Carbon fiber fabrication

Precursor fiber spinning. Lignin was spun into fibers using a homemade wet spinning unit (Fig. 2). Lignin powders were firstly mixed with PAN at a weight ratio of 1 : 1, and then the mixture was dissolved in *N*,*N*-dimethylformamide (DMF) at 60 °C with the concentration of 10%. Lignin/PAN dopes were sonicated using a Branson 1510 sonicator for 2 h before spinning to remove existing air bubbles. The dopes were then injected into a methanol coagulation bath (−20 °C) at a rate of 0.08 mL min^{-1} to form fibers. The as-spun fibers were wound onto a rolling drum. After washing with deionized water, the fibers were cut and hung under 15 g load until dry.

To evaluate the impact of different lignin-to-PAN ratios on the properties of the resultant fiber, lignin extracted from hardwood was mixed with PAN at two additional ratios of 65 : 35 and 75 : 25 with higher lignin content in the spinning dopes. Other conditions for wet spinning of the lignin/PAN dopes at 65 : 35 and 75 : 25 ratios were the same as that of the lignin/PAN ratio at 1 : 1 (or 50 : 50).

Thermostabilization and carbonization. The as-spun lignin precursor fibers were thermostabilized and then carbonized into carbon fibers. The thermostabilization was carried out using a muffle furnace (GSL 1200X, MTI Corporation, Richmond, CA) at atmospheric pressure. The heating was from room temperature to 250 °C at a heating rate of 1 °C min^{-1}. The holding time at 250 °C was 1 h. The thermostabilized fibers then underwent carbonization in a split tube furnace with a vacuum system under a nitrogen atmosphere (240 cm^3 min^{-1}) (GSL 1600X, MTI Corporation, Richmond, CA). The temperature for carbonization was increased from room temperature to 1000 °C with a heating rate of 5 °C min^{-1} and holding at 1000 °C for 1 h.

2.4 Carbon fiber characterization

Field emission scanning electron microscope (FE-SEM). The morphologies of carbon fibers were observed under a Quanta 600F FE-SEM (FEI Company, Hillsboro, OR). Carbon fibers were coated with 10 nm iridium (Ir) prior to the observation. The working distance was 10 mm, and the accelerating voltage applied was 5 kV. To obtain the morphologies of carbon fiber cross-sections, the fibers were mounted vertically on the SEM sample holder and then observed using a FE-SEM under the same conditions.

High-resolution transmission electron microscopy (HR-TEM). TEM samples were prepared using a Tescan LYRA-3 Model GMH Ga^+ Focused Ion Beam Microscope with a standard FIB lift-out technique. The ion (Ga^+) beam operated at 30 kV with a beam current ranging from 3 nA down to 1 nA was used to thin the membrane down to about 1 μm. The sample was further polished to 1100 nm using successive currents of 1000, 300, and 100 pA followed by final polish at 5 kV and 40 pA. HR-TEM was performed with an aberration-corrected scanning transmission electron microscope (S/TEM, Thermo Fisher Titan Themis Z 300) operated at 200 kV with a convergence semi-angle of 23.6 mrad. The microscope was aligned before every experiment using a gold standard sample. The microscope was set to the C2 aperture at 50 μm with the beam current set between 150 and 200 pA during the data acquisition.

Differential scanning calorimetry (DSC). DSC was performed using a TA Q2500 system (TA Instruments, New Castle, DE) with two heating cycles under a nitrogen atmosphere. Five milligrams of thermostabilized fibers were placed in a pan and then heated from 0 °C to 400 °C. Both heating and cooling rates were 10 °C min^{-1}. The glass transition temperature (T_g) was derived from the second cycle of DSC analysis. All DSC thermograms are shown in Fig. S4.†

Tensile test. The mechanical performances of carbon fibers were measured under a TestResources universal mechanical tester (Shakopee, MN). A 2 N load cell with the resolution of 0.0001 N was used. The fibers were mounted on a sample holder made of paper board with the help of super glue. The sample holder was then fixed on two grippers. For the measurement, the displacement rate was set at 0.200 mm min^{-1}. The applied force (F) and the corresponding displacement (d) were monitored synchronously during the measurement. The original length (L) of fibers was measured using a vernier caliper. To obtain the area (A) of each fiber, the morphologies of the cross-sections of carbon fibers were observed under the aforementioned FE-SEM after the test. The area was then calculated using the software ImageJ®. Stress–strain curves can be plotted after getting stress (σ) and strain (ε) using the equations of $\sigma = F/A$ and $\varepsilon = d/L$, respectively. The tensile strength represented the maximum stress at fracture and the modulus of elasticity (MOE) was obtained from the slope of the elastic deformation region in a stress–strain curve.

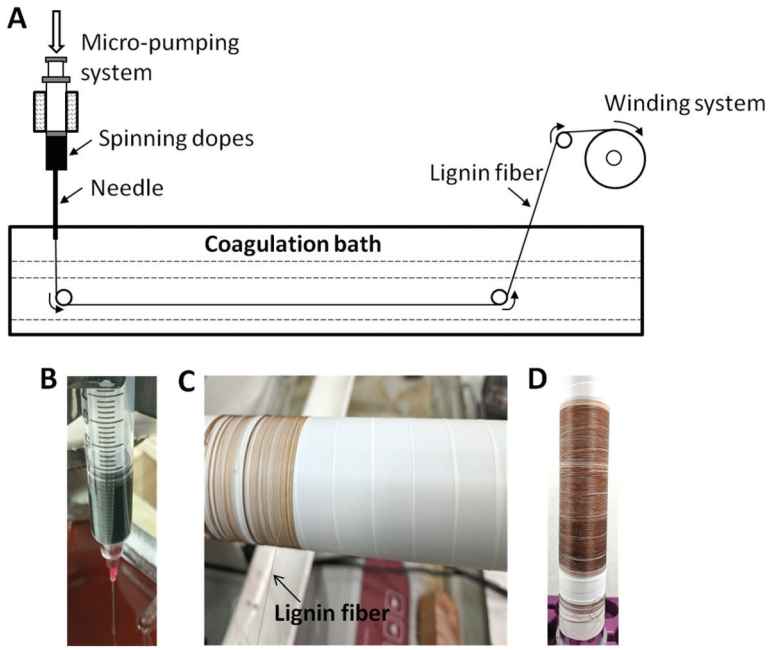

Fig. 2 Lignin fiber spinning setup. (A) Spinning dopes were extruded using a micro-pump through a needle immersed in a coagulation bath, and the formed fiber was continuously collected on the winding drum. (B) Close-up view of the fiber formation, where the lignin fiber was pulled out when lignin solution was pumped into a methanol/DMF coagulation bath. (C) A single fiber out of the coagulation bath was collected on the winding drum. (D) The collected as-spun lignin fibers.

Elongation (%) was calculated from $d'/L \times 100$, where d' is the displacement at the fracture. For each sample, at least 15 fibers were measured to obtain an average result.

Electrical conductivity measurement. The electrical conductivity of the carbon fibers was measured using a Fluke 87 TRUE RMS multimeter. The measurement was as shown in Fig. 4B. A single fiber was fixed with silver paint (GC Electronics) onto a cover glass, and then the electrical resistance (R, Ω) of the fibers between two silver paints was measured with a multimeter at ambient atmosphere. The electrical conductivity (σ, S m^{-1}) was calculated from the equation of $\sigma = 1/\rho = L/(R \times A)$, where ρ is electrical resistivity (Ω m), and L (m) and A (m^2) are the length and the cross-section area of the fiber as measured, respectively. The length (L) of the fiber was measured using the aforementioned vernier caliper. To calculate the area (A) of the fiber cross-section, the diameter of each fiber was measured under a Zeiss Axiophot microscope after the conductivity test, and at least 25 points on one fiber were measured to give an average fiber diameter.

X-ray diffraction (XRD). XRD analysis of carbon fiber crystallite structures was performed under a Bruker D8 Discovery XRD (Bruker, Madison, WI). To avoid the orientation preference, carbon fibers were ground into fine powders using an agate mortar and pestle before the measurement. An X-ray resource was generated at 40 kV voltage and 40 mA current with a Cu Kα wavelength (λ) of 1.542 Å. The scanning range (2θ) was from 8° to 55°, the scanning step size was 0.05°, and the scanning rate was set at 1.5° min^{-1}. The crystalline size (L_{hkl}) was calculated from the Scherrer equation: $L = \frac{K\lambda}{\beta \cos \theta}$, where L is the crystalline size (nm); K is the shape factor, set as 0.94 in this calculation; λ is the X-ray wavelength (1.542 Å); β is the full width at half maximum (FWHM) in radian; θ is the Bragg angle in degrees. The distance between two crystalline lattices (d_{hkl}) was estimated using Bragg's law: $2d \sin\theta = n\lambda$, where d is the distance in nm; θ is the Bragg angle in degrees; n is set as 1.

Raman spectroscopy. The ground carbon fiber powder was mounted on a glass slide with the help of double adhesive tape, and Raman spectra were obtained under a Horiba Jobin–Yvon LabRam Raman Confocal Microscope with a 633 nm laser, 10× magnification of objective lens,a D0.3 filter, 200 μm confocal pinhole, 10 s exposure time, and 10 accumulations. The D band (1348 cm^{-1}) and G band (1581 cm^{-1}) were deconvoluted by the Guassian curve fitting method using Origin 9 software. The G/D ratios were calculated from the area ratios of these two bands.

3. Results and discussion

3.1. Manufacturing carbon fibers from lignin derived from various biomass feedstocks after mixing with PAN

In order to explore the impacts of the lignin structure *in planta* on the carbon fiber performances, lignin from various types of feedstocks with different biomass characteristics was extracted

and then mixed with PAN for manufacturing carbon fibers. Corn stover, switchgrass, loblolly pine, red cedar and sugar maple all have been extensively utilized as biomass feedstocks in both biorefinery and the pulping industry,[30] and they were selected in this research as representative feedstocks of herbaceous plants, softwood and hardwood, respectively (Fig. 1). As an organosolv method, acetic acid extraction has been employed to fractionate lignin from these biomass samples. Acetic acid extraction has the advantages of relatively mild reaction conditions at atmosphere pressure and lower temperature (around 118 °C, see the Experimental section), as well as the high purity of the lignin products as indicated by the low ash content (Table S2†). Moreover, acetic acid lignin has been used to fabricate carbon fibers[36,37] and activated carbon fibers[38] in established studies, proving the reliability of this lignin extraction for carbon fiber manufacturing.

To prepare lignin fibers, lignin extracted from these five feedstocks was mixed with PAN at a 1 : 1 weight ratio and then dissolved in DMF to render a spinning dope with 10% concentration. A single fiber was formed under a customized wet-spinning setup (Fig. 2A), where spinning dopes were injected into a methanol coagulation bath (Fig. 2B) and then the formed single fibers were collected on a winding drum (Fig. 2C and D). As shown in Fig. 2D, the as-spun precursor fibers had a brownish color and were well aligned on the collection drum. The continuous length of the as-spun fibers can reach 300 meters, indicating the stability and reliability of the spinning technology. Moreover, we evaluated the fiber performance for lignin-to-PAN ratios from 1 : 1 (or 50% : 50%) to 65% : 35% and 75% : 25% in order to evaluate if more PAN could be replaced by lignin. The increased lignin content led to deteriorated spinnability and decreased quality of the as-spun fibers (as shown in Fig. S6†), indicating that the lignin-to-PAN ratio at 1 : 1 was optimal for replacing lignin with PAN for carbon fiber manufacturing. The precursor fibers were subsequently subjected to thermostabilization at 250 °C and thereafter carbonization at 1000 °C to convert into carbon fibers. The morphologies of the carbon fibers were analyzed using a scanning electron microscope (SEM). Several aspects of morphological features indicated the robustness and reliability of the manufacturing process.

First, morphological analysis of the prepared lignin-based carbon fibers showed high quality in terms of fiber geometrical structures. As shown in Fig. 3A1–E1, each lignin-derived carbon fiber was well separated with the same oriented directions. Even though the surfaces of the carbon fibers had some indents along fibers (Fig. 3A2–E2), which could be rendered by polymer coagulation processed on the interfaces between the spinning dopes and the coarse interior faces of the injection needle, the cross-sections of all carbon fibers were smooth and non-porous according to SEM analysis (Fig. 3A3–C3). These results suggested that the polymers of lignin and PAN were coagulated and interacted intimately with each other without significant void-defect formation in the coagulation process.[39,40] In addition, all carbon fibers had similar average diameters of around 36 μm (Fig. 3A4–E4), indicating the consistency of the resultant fibers and the stability and replicability of the customized wet-spinning system. More importantly, unlike the previous lignin carbon fibers made by electrospinning,[11] each carbon fiber prepared through wet spinning was uniform in the fiber axial direction and free of bead defects (Fig. 3), suggesting the robustness of this customized wet spinning technology. All these data of morphological analysis showed that the carbon fibers had homogeneous geometrical structures.

Second, the diameter distribution analysis suggested that the carbon fibers from different feedstocks showed notable variations in spinnability, among which lignin from hardwood biomass showed the best spinnability. As shown in the histograms in Fig. 3A4–E4, carbon fibers made of lignin from sugar maple had a narrower diameter distribution (ranging from 34 to 40 μm, Fig. 3E4) than that of red cedar (ranging from 32 to 40 μm, Fig. 3D4) and other biomass (loblolly pine, switchgrass and corn stover, ranging from 32 to 42 μm, Fig. 3A4–3C4, respectively). In addition, the percentage for the most frequent 2 μm diameter range was 65.0% for the carbon fibers made from the lignin of sugar maple (Fig. 3E4), which was much higher than those made from all other lignins of red cedar (50.0%, Fig. 3D4), loblolly pine (35.0%, Fig. 3C4), switchgrass (40.0%, Fig. 3B4) and corn stover (37.5%, Fig. 3A4). These results highlighted that lignin from sugar maple could improve the spinnability of the lignin, and thereby the uniformity in the diameters of carbon fibers. The improved spinnability could be attributed to lignin chemical structures and could correlate with the enhanced performances of carbon fibers, such as mechanical properties and electrical conductivity. We thereafter evaluated the carbon fiber performances and explored the relationship between lignin chemistry and lignin carbon fiber properties.

3.2. Mechanical properties of lignin-based carbon fibers from various biomass feedstocks

Current lignin-based carbon fibers have significantly lower mechanical performances as compared to the traditional PAN-based carbon fibers, which could be attributed to the chemistry of the carbon fiber precursor. A tensile test revealed that the carbon fibers derived from sugar maple lignin had superior mechanical performances, which were even comparable to pure PAN-based carbon fibers. As shown in Fig. 4A-a, the tensile test showed linear stress *versus* strain curves of lignin-based carbon fibers, and revealed elastic deformation behaviors of the carbon fibers before ultimate fracture.[41] From the stress–strain curves, the modulus of elasticity (MOE, Fig. 4A-b) and tensile strength (Fig. 4A-c) were calculated from the slope of the elastic deformation region and the stress at ultimate fracture, respectively. As shown in Fig. 4A-b, the MOE of carbon fibers showed significant differences among hardwood, softwood, and herbaceous biomass. In particular, the MOE of the carbon fibers made of lignin from sugar maple (hardwood) was 40.4 GPa, which was higher than those of carbon fibers made of lignin from both red cedar (37.7 GPa) and loblolly pine (36.2 GPa) (softwoods) and was much higher

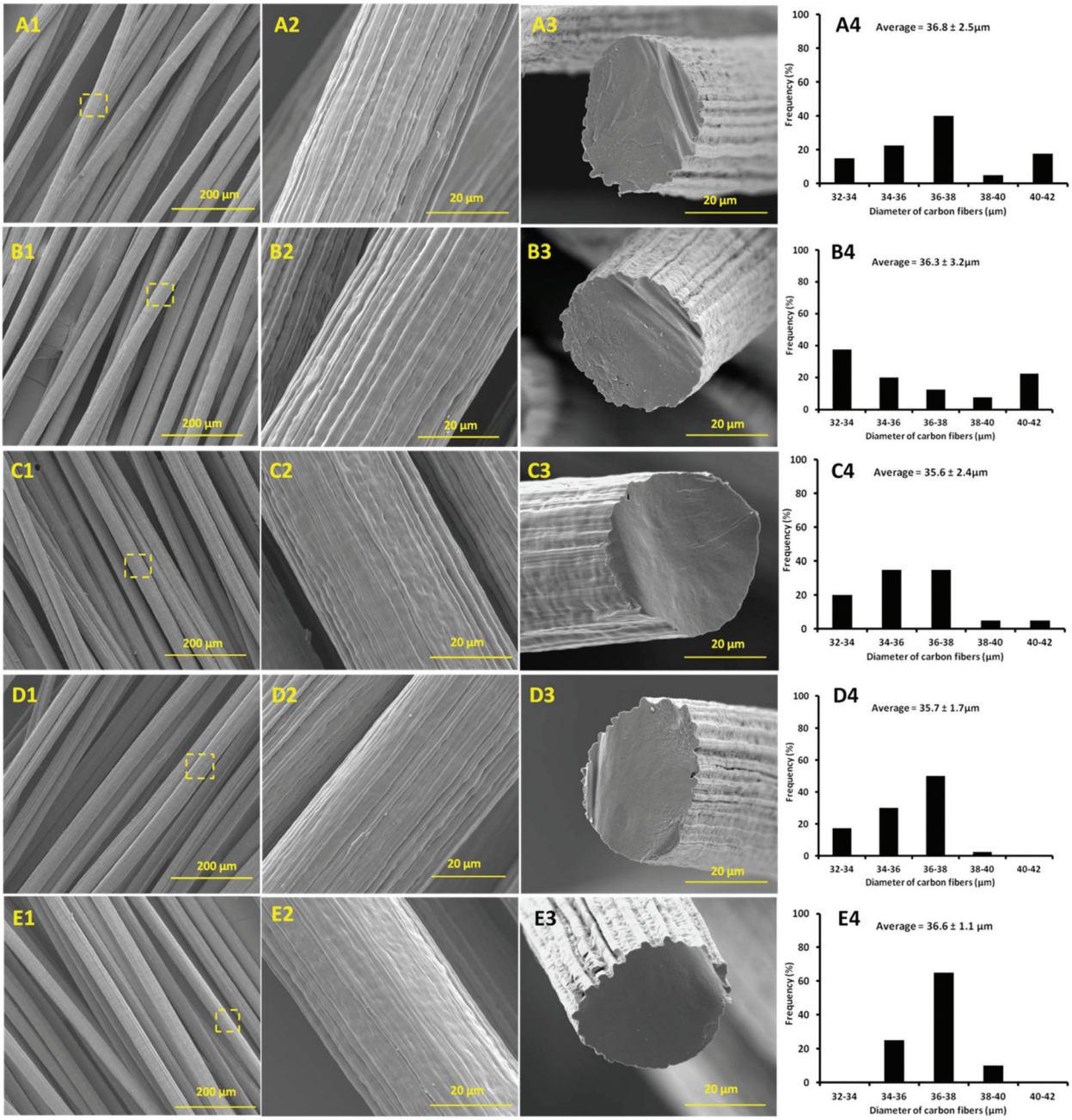

Fig. 3 SEM images of the surfaces and cross-sections of carbon fibers. Panels A, B, C, D and E are corn stover, switchgrass, loblolly pine, red cedar and sugar maple, respectively. The histograms in Panel 4 are the diameters and diameter distributions of carbon fibers.

than those of switchgrass (33.8 GPa) and corn stover (28.5 GPa) (herbaceous plants). Meanwhile, the tensile strength of carbon fibers made of sugar maple lignin (475 MPa) (hardwood) was about 1.2-fold higher than those made of red cedar lignin (404 MPa) and loblolly pine lignin (396 MPa) (softwood), and was 1.6- and 2.6-fold higher than those made of switchgrass lignin (299 MPa) and corn stover lignin (182 MPa) (herbaceous plants), respectively (Fig. 4A-c). In addition, the elongation of lignin-based carbon fibers increased from 1.07% and 1.15% for corn stover and switchgrass, respectively, to 1.35% and 1.45% for loblolly pine and red cedar, respectively, and further increased to 1.51% for sugar maple (Fig. 4A-d).

More importantly, the sugar maple lignin-derived carbon fibers even exhibited comparable mechanical properties to those of the pure PAN-based carbon fibers. As shown in Fig. 4A-b–d, the MOE of a pure PAN-based carbon fiber was 40.5 GPa, which was similar to that of the sugar maple lignin-based carbon fiber (40.4 GPa). Both tensile strength (453 MPa) and elongation (1.40%) of the PAN-based carbon fiber were actually slightly lower than those of the sugar maple lignin-

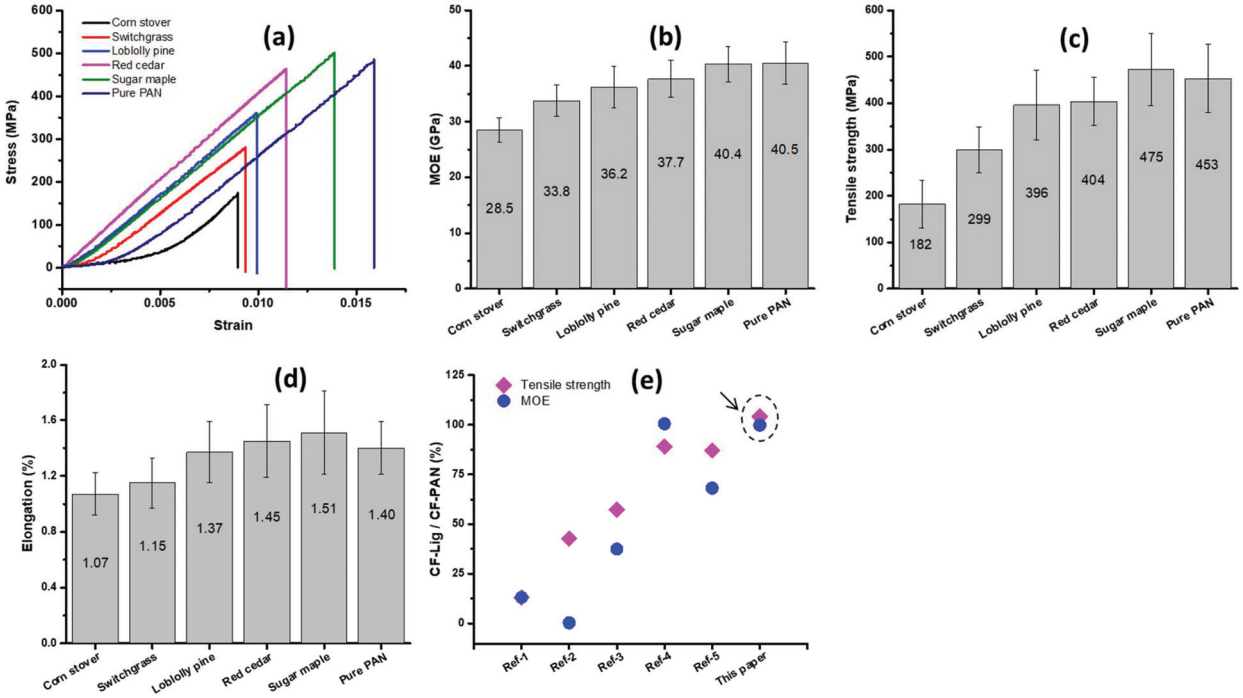

Fig. 4 Mechanical properties of lignin-based carbon fibers. (a) Representative stress–strain curves of carbon fibers; (b) modulus of elasticity (MOE); (c) tensile strength; (d) elongation; (e) the comparison of the lignin-based carbon fiber (CF-Lig) with the pure PAN carbon fiber (CF-PAN) as obtained in this study and reported in other studies. In the Panel e, the *Y*-axis CF-Lig/CF-PAN represented the percentage of CF-Lig mechanical properties to that of the CF-PAN, and the *X*-axis ref. 1–5 were Lin *et al.* (2012), Thunga *et al.* (2014), Ding *et al.* (2016), Liu *et al.* (2017), and Jin *et al.* (2018), respectively, which are given in Table S5.† The arrow and dashed circle highlight our data. The calculations of the data in Panel e are also given in Table S5.†

based carbon fiber. As compared to previous studies, for the lignin-based carbon fiber compared with the pure PAN-based carbon fiber prepared under the same thermostabilization and carbonization conditions, the sugar maple lignin-based carbon fiber in this study represented the lignin-based fibers with the best comparable performance to pure PAN-based carbon fibers (Fig. 4A-e and Table S5†). All of these results suggested that carbon fibers made of lignin from hardwood have better mechanical properties than those from softwood and herbaceous plants. The tensile test indicated that lignin from different types of biomass could significantly impact carbon fiber mechanical performances.

3.3. Electroconductive properties of lignin-based carbon fibers from different biomass feedstocks

The electrical conductivity of the resultant carbon fibers correlated with their mechanical performances. As shown in Fig. 5a, a single carbon fiber was used as a resistance in an electrical loop to test its electrical conductivity. The carbon fiber was fixed on a cover glass with silver paint. When 3 V voltage was applied, the bulbs connected to the lignin carbon fiber derived from all biomass feedstocks can be lighted (Fig. 5-b1–b5). Nevertheless, the brightness of the lighted bulb increased in the order of corn stover, switchgrass, loblolly pine, red cedar and sugar maple (Fig. 5-b1–b5). These results highlighted that carbon fibers made from sugar maple lignin had the best electrical conductivity as compared to those from other feedstocks. When the voltage was increased to 4.5 V, the bulb connected to the carbon fiber made of sugar maple lignin became much brighter as compared with 3 V voltage applied (Fig. 5-b6). In order to further understand the mechanisms underlying the differential electroconductivity, we tested the electrical conductivity of the fibers before carbonization. The electrical conductivity of the thermostabilized fiber from sugar maple lignin was further visualized by lighting a bulb at 4.5 V voltage. As shown in Fig. 5-b7, the bulb was completely off, indicating that thermostabilized lignin polymers by themselves were electrical resistant. These data highlighted that the improved electrical conductivity of sugar maple lignin-based carbon fibers could have resulted from the enhanced carbon structures during the carbonization process.[42] In fact, the electrical conductivity of the carbon fiber made from sugar maple lignin was 14 225 S m^{-1} as measured using a multimeter, which was higher than those of the carbon fibers made from both red cedar (13 909 S m^{-1}) and loblolly pine lignin (13 071 S m^{-1}), and was much higher than those made of both switchgrass (9405 S m^{-1}) and corn stover lignin (6585 S m^{-1}) (Fig. 5c). The study again demonstrated that the sugar maple (hardwood) lignin-based carbon fiber shows the most improved electrical conductivity as compared to those based on lignin from softwoods and herbaceous plants. Moreover, the enhanced electroconductive properties

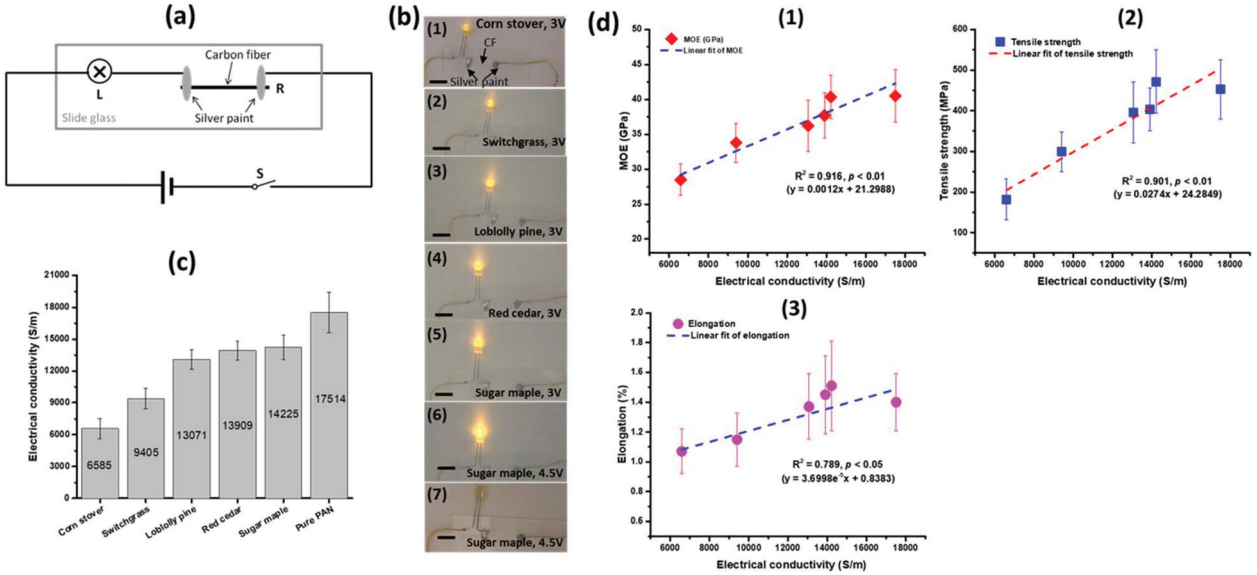

Fig. 5 Electrical conductivity of lignin-based carbon fibers. (a) Lignin carbon fiber as a resistance in the circuit; (b) the bulbs lighted at different voltages with carbon fibers as resistances; b-1 to b-5 were lighted at 3 V, which were derived from corn stover, switchgrass, loblolly pine, red cedar and sugar maple, respectively; b-6 was the sugar maple lignin carbon fiber lighted at 4.5 V. The thermostabilized fiber of lignin from sugar maple was used as control (b-7); (c) the electrical conductivity of lignin-based carbon fibers as measured with a multimeter; (d) linear correlation between electrical conductivity and mechanical performances. d1 to d3 are correlations of electrical conductivity with MOE, tensile strength, and elongation, respectively.

of the lignin carbon fiber were consistent with its enhanced mechanical properties. As shown in Fig. 5d, a linear regression model revealed the good correlation between the electrical conductivity and MOE (R^2 = 0.916, p < 0.01), tensile strength (R^2 = 0.901, p < 0.01), and elongation (R^2 = 0.789, p < 0.05), indicating that the electroconductive performance of carbon fibers can be improved synergistically with the mechanical properties. The mechanistic study of these improvements was subsequently carried out by analyzing the crystallite carbon structure in lignin-based carbon fibers.

3.4. Microstructure of the lignin carbon fiber determines the mechanical and electroconductive properties

The crystallite in lignin-based carbon fibers had been characterized as a pre-graphitic turbostratic carbon structure,[7,11] which was mainly comprised of more or less bent crystallite layers with sp^2-hybridized carbon atoms.[43] The size and the content of the crystallite carbon in carbon fibers were analyzed using both X-ray diffraction (XRD) and Raman spectroscopy. First, XRD analysis revealed the improved crystallite size (L_{hkl}) in the carbon fibers made of sugar maple (hardwood) lignin as compared to other feedstocks. As shown in Fig. 6A, the XRD diffractograms of all-lignin carbon fibers showed main peaks around the 2θ of 23.5°, displaying the reflection at the (002) plane.[44] The thickness of the crystallite was calculated using Scherrer's equation. As shown in Fig. 6B, the crystallite size for the carbon fiber made of the sugar maple lignin was 1.256 nm, which was higher than those made from red cedar lignin (1.156 nm) and loblolly pine lignin (1.001 nm), and was much higher than that made from switchgrass lignin (0.971 nm) and corn stover lignin (0.894 nm). These data highlighted that carbon fibers made from hardwood lignin had a larger crystallite size than those made from softwood and herbaceous plants. Second, Raman spectroscopy analysis further confirmed that the carbon fibers made from sugar maple (hardwood) lignin had increased pre-graphitic turbostratic carbon structures as compared to those from the softwood and herbaceous feedstocks. As shown in Fig. 6C, besides the disordered D band carbon structure at around 1325 cm^{-1}, all lignin-based carbon fibers had clear G bands at around 1586 cm^{-1}, indicating the existence of the graphite-derived carbon structures.[7,11] The integrated G/D ratio as shown in Fig. 6D was 0.565 for the carbon fiber made from sugar maple lignin, whilst the G/D ratio was 0.526 and 0.498 for carbon fibers made from red cedar and loblolly pine lignin and 0.419 and 0.340 for carbon fibers made from switchgrass and corn stover, respectively. The increased G/D ratio in the lignin carbon fiber suggested the increased content of the pre-graphitic turbostratic carbon structure.[11] However, the turbostratic carbon structure was observed under HR-TEM for the pure PAN carbon fiber but was not found for hardwood lignin/PAN-based carbon fibers (Fig. S7†), which could be attributed to the very small size of the crystalline structures as characterized by XRD. Overall, the crystallite structure analysis by XRD and Raman spectroscopy revealed the enhanced turbostratic carbon structure in carbon fibers made of hardwood lignin as compared to softwood and herbaceous plants.

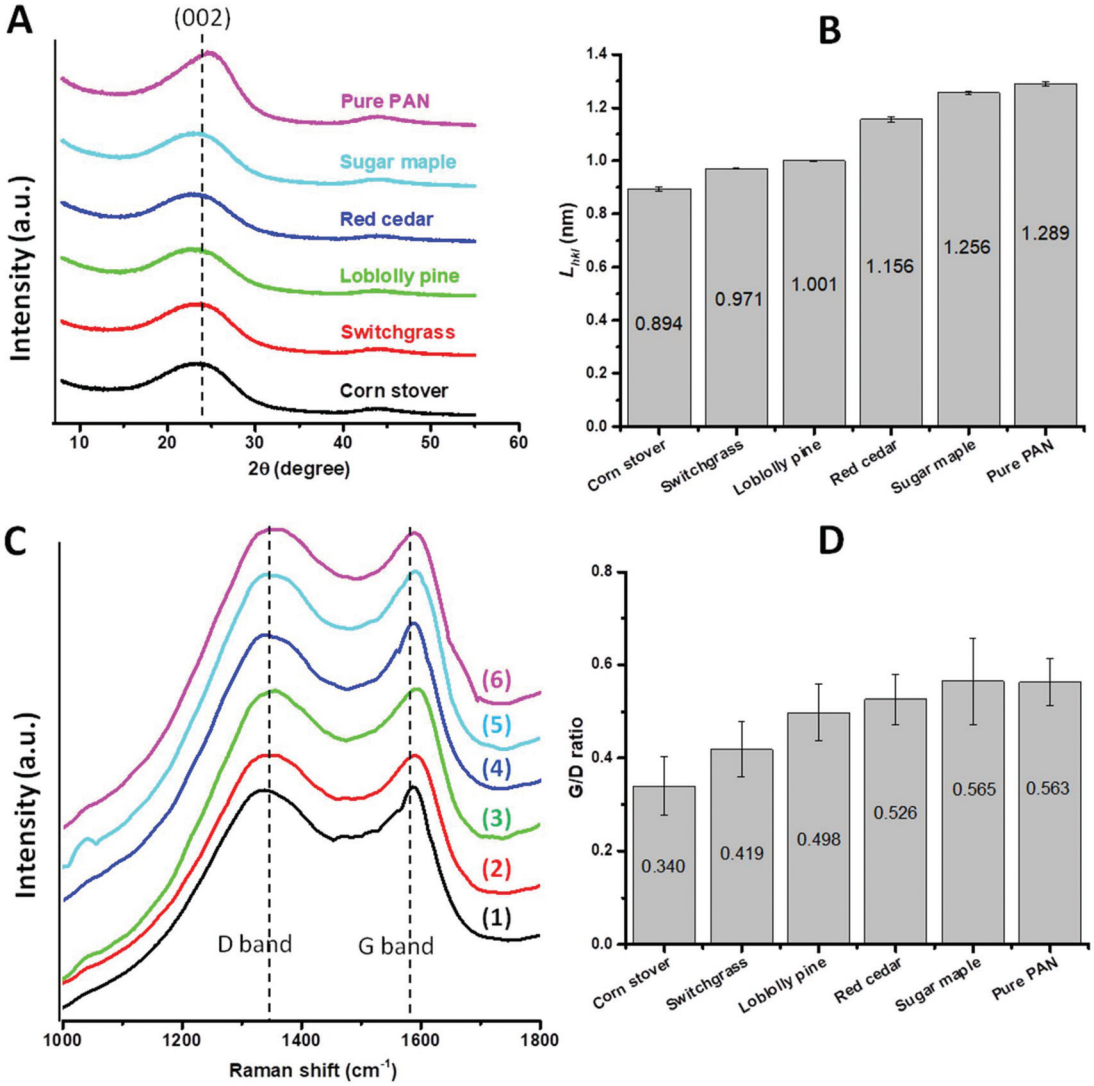

Fig. 6 Characterization of the crystallite structures in carbon fibers by XRD (A and B) and Raman microscopy (C and D). (A) XRD diffractograms of carbon fibers made of lignin derived from different biomass feedstocks and pure PAN; (B) the crystallite size (L_{hkl}) in carbon fibers as calculated from the Scherrer equation; (C) Raman microscopy spectra of carbon fibers, where C1–C6 were corn stover, switchgrass, loblolly pine, red cedar, sugar maple and pure PAN, respectively. The left peak in panel C around 1330 cm^{-1} represents the D band, and the right peak around 1595 cm^{-1} is the G band; D, the G/D ratios of carbon fibers as calculated from the G and D bands from Raman microscopy.

The results highlighted several mechanistic discoveries that could guide the future development of multi-functional lignin carbon fibers of high quality. First, microstructures define the quality of carbon fibers. The best-performing mechanical properties and electrical conductivity of the carbon fibers made from the sugar maple lignin could be attributed to the best turbostratic carbon structures as revealed by XRD and Raman spectroscopy. In other words, the enhanced microstructures could account for the superior mechanical and electroconductive properties of carbon fibers made from hardwood lignin. Second, the mechanical and electroconductive performance of carbon fibers can be improved synergistically based on the enhanced microstructure. The results thus highlighted that the improvement of the microstructure could be a universal approach to synergistically improve different properties of lignin-based carbon fibers. Third, the synergistic improvement of both mechanical properties and electrical conductivity for hardwood lignin-derived carbon fibers indicated that hardwood lignin could serve as a superior precursor for multi-functional renewable carbon materials. Overall, the carbon fibers made of hardwood (sugar maple) lignin had the best crystallite structure and performances as compared to those made of lignin from softwoods (red cedar and loblolly pine) and herbaceous plants (switchgrass and corn stover). The results opened an new avenue to further study what biomass characteristics could define the microstructure of lignin

carbon fibers and therefore improve their multi-functional properties.

3.5. Explorative study revealed that *β-O*-4 linkages boost lignin carbon fiber performances

The diverse mechanical and electroconductive properties for carbon fibers from various biomass feedstocks with differential lignin characteristics allowed us to identify the key lignin chemical features defining the carbon fiber performance. Such a fundamental study will guide the future feedstock and process development to deliver high-quality carbon fibers. In order to better understand how lignin chemistry and biomass characteristics define the lignin carbon fiber performance, comprehensive analyses of the interunitary linkages and monolignol composition derived from various biomass feedstocks were carried out using 2D HSQC NMR.

Lignin in hardwood, softwood and herbaceous plants had different interunitary linkage profiles, partially resulting from different S, G and H units.[19] Using the 2D HSQC NMR technique, we have clearly observed the difference in the frequencies of *β-O*-4, *β*-5 and *β–β* linkages among different types of biomass (Fig. 7). As displayed in Fig. 7A and Table S1,† carbon-*α* in *β-O*-4, *β*-5 and *β–β* was assigned to the peaks around δ_C/δ_H 71.5/5.0 ppm, δ_C/δ_H 87.7/5.5 ppm and δ_C/δ_H 85.0/4.7 ppm, respectively.[11,35] The frequencies of the linkages were expressed as per 100 aromatic rings of S, G, and H units, which were assigned to the peaks at around δ_C/δ_H 103.8/6.70 ppm ($S_{2/6}$), δ_C/δ_H 111.3/6.80 ppm (G_2) and δ_C/δ_H 127.2/7.30 ppm ($H_{2/6}$), respectively (Fig. S1† and Table S1†).[35] As shown in Fig. 7B1, the main *β-O*-4 linkage (β-aryl ether) was higher in sugar maple (35.8%) than those in both red cedar (31.6%) and loblolly pine (30.1%), and was much higher than that in switchgrass (26.9%) and corn stover (21.2%). Meanwhile, *β*-5 linkages (phenylcoumaran, in Fig. 7B2) were significantly higher in lignin from both red cedar (20.78%) and loblolly pine (21.02%) than those from sugar maple (5.00%), switchgrass (4.58%) and corn stover (5.41%). The difference of *β*-5 among lignin from the latter three biomasses was not significant. In addition, the content of *β–β* linkage was much lower than those of both *β-O*-4 and *β*-5 in all types of lignin. The *β–β* linkage content in red cedar (1.28%), loblolly pine (1.23%), and switchgrass (1.58%) was higher than those from the corn stover and sugar maple. These results of the high *β-O*-4 and low *β*-5 in sugar maple lignin were not out of expectation. As compared to the predominant G unit content in softwood (*e.g.*, loblolly pine and red cedar) lignin, hardwood lignin from the sugar maple had most S units with methoxyl on the carbon-5 (C_5) position (Fig. S1†). The higher S unit content could prefer R_β and $R_{O\text{-}4}$ radical formation during radical coupling (Fig. S5A and S5B-a†), attributed to the higher *β-O*-4 frequency in the sugar maple lignin. Interestingly, both herbaceous plants (*e.g.*, switchgrass and corn stover) had significantly higher S unit content, yet lower *β-O*-4 frequency than that of softwoods (loblolly pine and red cedar) (Fig. 7B1 and S1A†). Such variations could be due to the impact of processing technologies on the ester linkage, instead of the content of a certain monolignol. The herbaceous plants have a significant amount of *p*CA and FA units (Fig. S1†), which can form liable ester linkages in lignin.[45,46] These liable ester linkages could be readily broken down under chemical processing like acetic acid extraction, rendering the decreased *β-O*-4 frequency in lignin extracted from the herbaceous plants. Similar results can be observed when comparing corn stover with switchgrass. Even though corn stover had higher S units than switchgrass (Fig. S1A†), the lower *β-O*-4 frequency in corn stover could be due to the higher content of *p*CA and FA units (Fig. 7B1 and

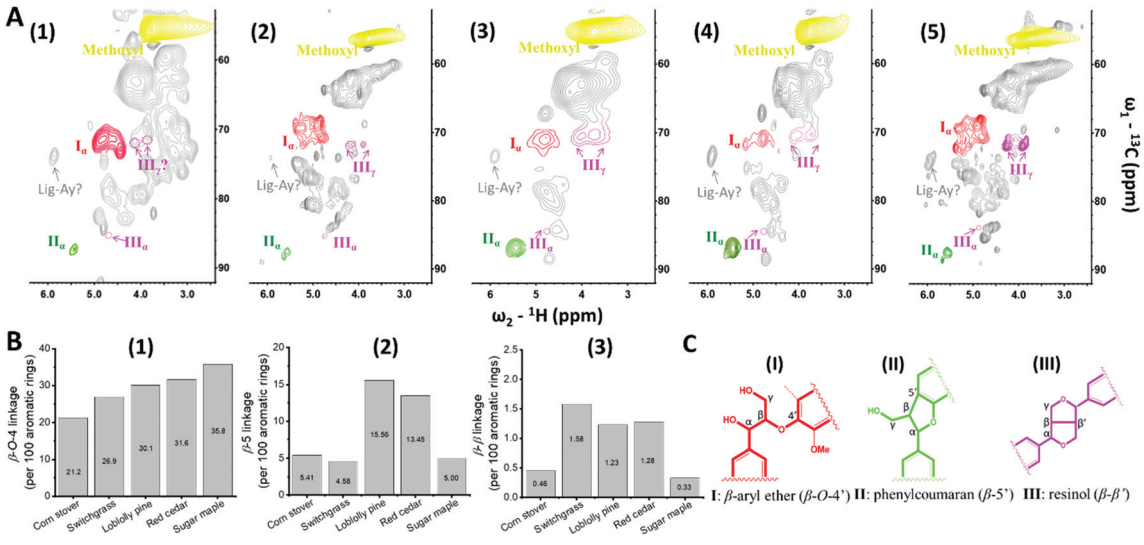

Fig. 7 Aliphatic regions of 2D ^{13}C–^{1}H (HSQC) NMR spectra. (A) Aliphatic regions of HSQC spectra, where the assigned lignin linkages are highlighted in different colors. A1, A2, A3, A4, and A5 are lignin from corn stover, switchgrass, loblolly pine, red cedar, and sugar maple, respectively; (B) the frequency of lignin linkages as measured by HSQC 2D NMR. B1, B2, and B3 are *β-O*-4, *β*-5, and *β–β* linkages, respectively, which were calculated based on 100 aromatic rings; (C) chemical structures of lignin linkages assigned in HSQC spectra. Lig-Ay, acetylated lignin that needs to be further confirmed.

S1A†). Meanwhile, high β-5 in red cedar and loblolly pine lignin (softwood) could result from its G units (Fig. S1†) with a vacant C_5 position, which could form more R5 radicals for β-5 radical coupling (Fig. S5B-b†). Overall, the frequencies of β-*O*-4 were found to be clearly different between various types of biomass, where hardwood lignin inherently had more β-*O*-4 than both softwood lignin and herbaceous plant lignin.

Traditionally, lignin content and composition were considered to be the key factors determining the biomass saccharification efficiency.[22] However, the biomass feedstock characteristics determining the quality of carbon fibers are largely un-defined. Our recent study suggested that different feedstock lines and growth conditions within the same species could impact molecular weight, polydispersity, and functional groups, all of which can contribute to carbon fiber performance.[47] Additionally, our previous studies of the fundamental structure–property relationship using fractionation technologies also revealed that lignin fraction with a smaller PDI (higher uniformity), higher molecular weight, more β-*O*-4 linkage, and less hydroxyl groups could correlate with higher mechanical properties of the resulting carbon fiber.[7,11,13,14] Nevertheless, it remains unclear how a particular feedstock species could make the structure beneficial for carbon fiber manufacturing. Notably, the molecular weight and PDI of the lignin samples from the five species showed no significant differences among them, proving a perfect reductionist system to investigate the impact of biomass characteristics other than molecular weight and uniformity on carbon material properties (Fig. S3 and Table S3†). We thereby carried out linear regression analysis of various carbon fiber properties in response to different biomass characteristics. Surprisingly, we have found that both mechanical properties (Fig. 8A) and electrical conductivity (Fig. 8B) correlated with the β-*O*-4 linkage profile. In particular, hardwood lignin with more β-*O*-4 linkages had higher mechanical properties (Fig. 4) and electrical conductivity (Fig. 5c). First, mechanical properties, in particular the MOE and tensile strength, fitted perfectly with the β-*O*-4 linkage in a linear regression model. As shown in Fig. 8A1 and A2, the linear regressions of β-*O*-4 *vs.* MOE and tensile strength resulted in the correlation determination (R^2) at 0.985 and 0.945, respectively, both of which had P values less than 0.01. Meanwhile, the linear regressions of β-*O*-4 *vs.* elongation had R^2 at 0.786 and $P < 0.05$ (Fig. 8A3). In addition, the linear regression of β-*O*-4 *vs.* electrical conductivity resulted in R^2 of 0.841 with $P < 0.05$ (Fig. 8B). These linear regression analysis results suggested that it is the lignin β-*O*-4 linkage that determines the multifunctional properties of lignin-based carbon fibers. Therefore, increasing the β-*O*-4 content boosted the performance of lignin-based carbon fibers, the MOE and tensile strength in particular.

Considering the increased crystallite carbon structures in carbon fibers as measured by XRD and Raman spectroscopy (Fig. 6), we further analyzed the correlation between β-*O*-4 linkages and carbon fiber crystallite structures. As shown in Fig. 8C, the β-*O*-4 linkage had a significant positive linear correlation with both the crystallite size (L_{hkl}, R^2 0.712 and $P <$

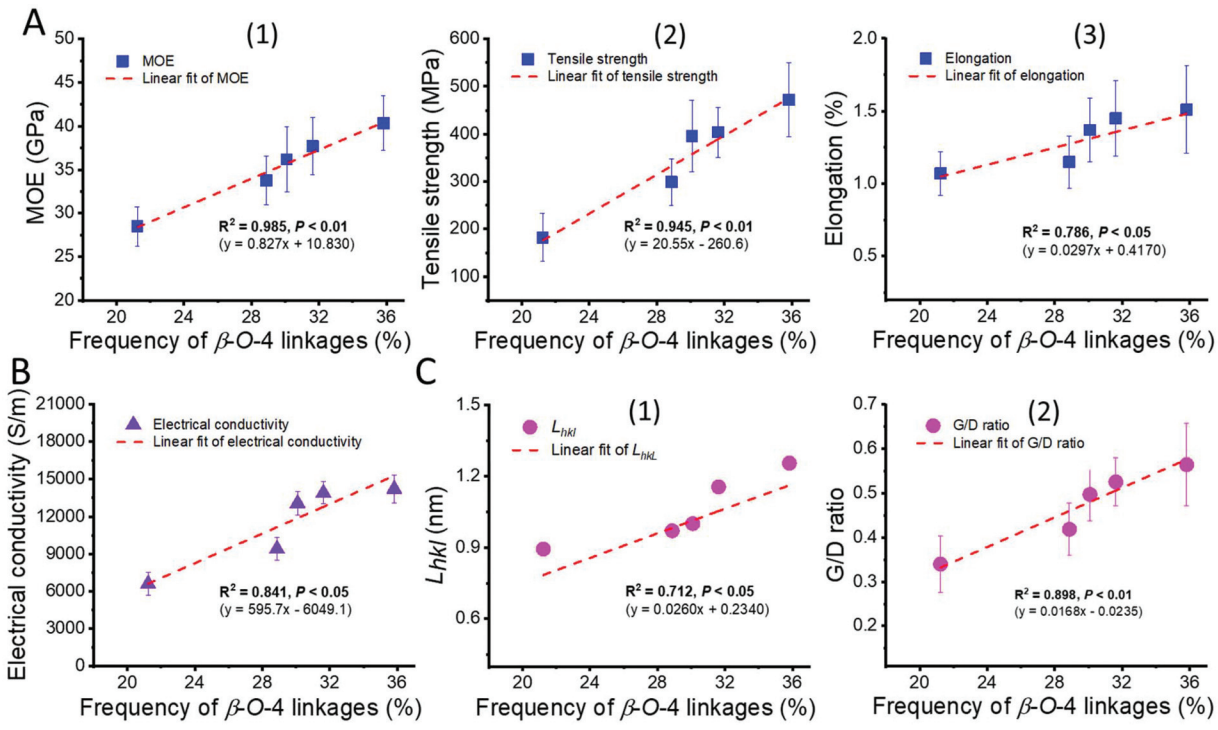

Fig. 8 The correlations of the lignin β-*O*-4 linkage with carbon fiber mechanical properties (A), electrical conductivity (B), and crystallite structures (C). A1, A2, and A3 in Pane A are correlations of the β-*O*-4 linkage with MOE, tensile strength, and elongation, respectively; C1 and C2 in Pane C are correlations of the β-*O*-4 linkage with L_{hkl} and G/D ratio, respectively.

0.05) and the crystallite content (G/D ratio, R^2 0.898 and $P < 0.01$), indicating that the *β-O*-4 linkage in the lignin polymer could enhance the crystallite formation, in particular forming more crystallite carbon structures. All of these results thus revealed that a lignin polymer with more *β-O*-4 linkages could enhance the crystallite formation and thereby boost the mechanical and electroconductive performances of the resulting carbon fibers.

The molecular mechanism through which *β-O*-4 linkages enhance the carbon fiber performance could lie in the flexibility of the lignin polymer chain.[48–50] Lignin with more *β-O*-4 linkages bonded by C–O–C uncondensed links could be more flexible. A lignin polymer with improved flexibility would result in better aligned polymer orientations under stretching force loaded on precursor fibers with a winding system during the coagulation process in wet spinning (see Fig. 2). Moreover, DSC analysis revealed that hardwood (sugar maple) lignin-based fibers had a lower glass transition temperature (T_g) than both softwood (red cedar and loblolly pine) and herbaceous plant (switchgrass and corn stover) lignin-based fibers (Fig. S4†), indicating the improved miscibility of lignin molecules with guest PAN molecules.[11,14] The improved miscibility also suggested that the *β-O*-4 linkage increased the flexibility of lignin polymers, as the aligned polymers with similar orientation could enhance the interactions between each other or with other guest polymers like PAN.[49] This improvement of lignin polymer orientations and polymer–polymer interactions in precursor fibers could enhance the formation of the pre-graphite turbostatic carbon structures in carbon fibers,[8,11,39] which would account for the boosted mechanical performance and electrical conductivity of carbon fibers.

In summary, using feedstocks with diverse biomass characteristics, we have defined the relationship between lignin chemistry and carbon fiber performance. Lignin polymers formed through different biosynthesis pathways in various biomass feedstocks with inherently different chemical features could be favorable for making quality carbon fibers with enhanced mechanical and electroconductive performances. Lignin structures with a high *β-O*-4 content could be manipulative through the regulation of the biosynthesis pathways, in particular the biosynthesis of monolignols.[51,52] This research thereby demonstrated that such manipulation of lignin engineering in biomass to regulate lignin structures toward favorable *β-O*-4 linkages for carbon fiber production could not only facilitate biomass processing, but also has the potential to transform the bioeconomy of lignocellulosic biorefinery and pulping mills by upgrading lignin byproducts into high-value products like carbon fibers.

4. Conclusion

Lignin carbon fibers are still struggling for commercialization due to their poor performance. In this study, we presented a new concept addressing this challenge where the quality of lignin carbon fibers can possibly be boosted through the regulation of lignin chemical structures in biomass feedstocks. The concept was built on the finding that hardwood (sugar maple) lignin with more *β-O*-4 linkages than both softwood (red cedar and loblolly pine) and herbaceous plants (switchgrass and corn stover) resulted in carbon fibers with enhanced mechanical properties and electrical conductivity. The fundamental understanding of why hardwood lignin leads to the best mechanical and electroconductive performances of carbon fibers was demonstrated by XRD and Raman spectroscopy, where the pre-graphite turbostractic carbon structures in carbon fibers made from hardwood lignin were significantly improved. Furthermore, the relationship between lignin linkages and carbon fiber performances was evaluated using scatter plots. The *β-O*-4 linkages in lignin showed significantly linear correlation with the crystallite structure and the performances of lignin-based carbon fibers, particularly the MOE and tensile strength. Such a correlation could guide the design of chemical processing of lignin molecular structures toward high-quality lignin-based carbon fibers. More importantly, the new concept presented in this research sheds light on lignin carbon fiber production where the regulation of lignin chemical structures through the manipulation of the lignin monolignol biosynthesis pathway *in planta* for high *β-O*-4 linkages could significantly boost carbon fiber performances. With the implementation of high *β-O*-4 linkages in lignin, the bioeconomy of both lignocellulosic biorefinery and the pulping industry could be thus transformed by concurrently maximizing the production of cellulose fibers and lignin-derived high-value carbon materials.

Author contributions

Q.L. and J.S.Y. designed the experiments. Q.L., C.H., M.L. and H.-S.L. carried out lignin extraction and fiber fabrication. Q.L. did lignin and the resulting carbon fiber characterization with the assistance of P.T. on DSC, W.W. on electrical conductivity measurement, and M.T.N. on HSQC. B.E.J. provided all wood samples for this research. Y.P. did GPC characterization. Y.P. and A.J.R. supervised Q.L. on all NMR analyses presented in this paper. J.L. helped Q.L. with FTIR characterization of all lignin samples. W.K. and S.X. did HR-TEM characterization of all carbon fibers. Q.L. and J.S.Y. discussed the results. Q.L. wrote the manuscript and J.S.Y. revised it. All authors contributed to the scientific discussions and comments on the manuscript.

Conflicts of interest

The authors declare no competing financial interests.

Acknowledgements

The authors would like to thank Dr Anup K. Bandyopadhyay in the Department of Materials Science and Engineering (MSEN),

Texas A&M University for his assistance with DSC and XRD characterization and Dr Thomas C. Stephens in Microscopy Image Center (MIC), Texas A&M University for his assistance with SEM. The authors also acknowledge the funding support of Texas A&M Energy Institute Seed Grant to J. S. Y. and DOE EERE BETO grants (DE-EE0007104, DE-EE0006112, and DE-EE0008250) to J. S. Y.

References

1 L. R. Lynd, *et al.*, How biotech can transform biofuels, *Nat. Biotechnol.*, 2008, **26**, 169.
2 N. Mosier, *et al.*, Features of promising technologies for pretreatment of lignocellulosic biomass, *Bioresour. Technol.*, 2005, **96**, 673–686.
3 C. E. Wyman, Biomass ethanol: Technical progress, opportunities, and commercial challenges, *Ann. Rev. Energy Environ.*, 1999, **24**, 189–226.
4 L. R. Lynd, J. H. Cushman, R. J. Nichols and C. E. Wyman, Fuel ethanol from cellulosic biomass, *Science*, 1991, **251**, 1318–1323.
5 V. Menon and M. Rao, Trends in bioconversion of lignocellulose: Biofuels, platform chemicals & biorefinery concept, *Prog. Energy Combust. Sci.*, 2012, **38**, 522–550.
6 F. Cherubini, The biorefinery concept: Using biomass instead of oil for producing energy and chemicals, *Energy Convers. Manage.*, 2010, **51**, 1412–1421.
7 Q. Li, *et al.*, Molecular weight and uniformity define the mechanical performance of lignin-based carbon fiber, *J. Mater. Chem. A*, 2017, **5**, 12740–12746.
8 D. A. Baker and T. G. Rials, Recent advances in low-cost carbon fiber manufacture from lignin, *J. Appl. Polym. Sci.*, 2013, **130**, 713–728.
9 Q. Li, J. A. Ragauskas and J. S. Yuan, Lignin carbon fiber: The path for quality, *Tappi J.*, 2017, **16**, 107–108.
10 H. Mainka, *et al.*, Lignin – an alternative precursor for sustainable and cost-effective automotive carbon fiber, *J. Mater. Res. Technol.*, 2015, **4**, 283–296.
11 Q. Li, *et al.*, Quality carbon fibers from fractionated lignin, *Green Chem.*, 2017, **19**, 1628–1634.
12 Q. Li, *et al.*, Microstructure defines the electroconductive and mechanical performance of plant-derived renewable carbon fiber, *Chem. Commun.*, 2019, **55**, 12655–12658.
13 Q. Li, *et al.*, Tuning hydroxyl groups for quality carbon fiber of lignin, *Carbon*, 2018, **139**, 500–511.
14 Q. Li, *et al.*, Non-solvent fractionation of lignin enhances carbon fiber performance, *ChemSusChem*, 2019, **12**, 3249–3256.
15 W. Boerjan, J. Ralph and M. Baucher, Lignin biosynthesis, *Ann. Rev. Plant Biol.*, 2003, **54**, 519–546.
16 N. Terashima and K. Fukushima, Heterogeneity in formation of lignin—XI: An autoradiographic study of the heterogeneous formation and structure of pine lignin, *Wood Sci. Technol.*, 1988, **22**, 259–270.
17 T. Higuchi, Lignin biochemistry: Biosynthesis and biodegradation, *Wood Sci. Technol.*, 1990, **24**, 23–63.
18 J.-K. Weng, X. Li, N. D. Bonawitz and C. Chapple, Emerging strategies of lignin engineering and degradation for cellulosic biofuel production, *Curr. Opin. Biotechnol.*, 2008, **19**, 166–172.
19 J. Ralph, *et al.*, Lignins: Natural polymers from oxidative coupling of 4-hydroxyphenyl-propanoids, *Phytochem. Rev.*, 2004, **3**, 29–60.
20 W. Jing-Ke and C. Clint, The origin and evolution of lignin biosynthesis, *New Phytol.*, 2010, **187**, 273–285.
21 R. Sibout and H. Höfte, Plant Cell Biology: The ABC of monolignol transport, *Curr. Biol.*, 2012, **22**, 533–535.
22 F. Chen and R. A. Dixon, Lignin modification improves fermentable sugar yields for biofuel production, *Nat. Biotechnol.*, 2007, **25**, 759.
23 C. G. Yoo, *et al.*, Significance of lignin S/G ratio in biomass recalcitrance of *populus trichocarpa* variants for bioethanol production, *ACS Sustainable Chem. Eng.*, 2018, **6**, 2162–2168.
24 V. A. Thomas, *et al.*, Comparative evaluation of populus variants total sugar release and structural features following pretreatment and digestion by two distinct biological systems, *Biotechnol. Biofuels*, 2017, **10**, 292.
25 S. D. Mansfield, K.-Y. Kang and C. Chapple, Designed for deconstruction – poplar trees altered in cell wall lignification improve the efficacy of bioethanol production, *New Phytol.*, 2012, **194**, 91–101.
26 R. Van Acker, *et al.*, Improved saccharification and ethanol yield from field-grown transgenic poplar deficient in cinnamoyl-CoA reductase, *Proc. Natl. Acad. Sci. U. S. A.*, 2014, **111**, 845–850.
27 S. K. Huntley, D. Ellis, M. Gilbert, C. Chapple and S. D. Mansfield, Significant increases in pulping efficiency in C4H-F5H-transformed poplars: Improved chemical savings and reduced environmental toxins, *J. Agric. Food Chem.*, 2003, **51**, 6178–6183.
28 A. Wagner, *et al.*, Syringyl lignin production in conifers: Proof of concept in a Pine tracheary element system, *Proc. Natl. Acad. Sci. U. S. A.*, 2015, **112**, 6218–6223.
29 R. Vanholme, B. Demedts, K. Morreel, J. Ralph and W. Boerjan, Lignin biosynthesis and structure, *Plant Physiol.*, 2010, **153**, 895–905.
30 2016 Billion-Ton Report. http://energy.gov/eere/bioenergy/2016-billion-ton-report.
31 S. Chatterjee, A. Clingenpeel, A. McKenna, O. Rios and A. Johs, Synthesis and characterization of lignin-based carbon materials with tunable microstructure, *RSC Adv.*, 2014, **4**, 4743–4753.
32 X. J. Ma, *et al.*, Lignin removal and benzene–alcohol extraction effects on lignin measurements of the hydrothermal pretreated bamboo substrate, *Bioresour. Technol.*, 2014, **151**, 244–248.
33 X.-J. Pan, Y. Sano, H. Nakashima and Y. Uraki, Atmospheric acetic acid pulping of rice straw (1) Pulping

conditions and properties of pulp, *Jpn. Tappi J.*, 1998, **52**, 408–415.
34 X. Pan and Y. Sano, Fractionation of wheat straw by atmospheric acetic acid process, *Bioresour. Technol.*, 2005, **96**, 1256–1263.
35 S. D. Mansfield, H. Kim, F. Lu and J. Ralph, Whole plant cell wall characterization using solution-state 2D NMR, *Nat. Protocols*, 2012, **7**, 1579–1589.
36 S. Kubo, Y. Uraki and Y. Sano, Preparation of carbon fibers from softwood lignin by atmospheric acetic acid pulping, *Carbon*, 1998, **36**, 1119–1124.
37 Y. Uraki, S. Kubo, N. Nigo, Y. Sano and T. Sasaya, Preparation of Carbon Fibers from Organosolv Lignin Obtained by Aqueous Acetic Acid Pulping, *Holzforschung*, 1995, **49**, 343–350.
38 Y. Uraki, A. Nakatani, S. Kubo and Y. Sano, Preparation of activated carbon fibers with large specific surface area from softwood acetic acid lignin, *J. Wood Sci.*, 2001, **47**, 465–469.
39 E. Frank, L. M. Steudle, I. Ingildeev, J. M. Sporl and M. R. Buchmeiser, Carbon Fibers: Precursor systems, processing, structure, and properties, *Angew. Chem., Int. Ed.*, 2014, **53**, 5262–5298.
40 J. P. Bell and J. H. Dumbleton, Changes in the structure of wet-spun acrylic fibers during processing, *Text. Res. J.*, 1971, **41**, 196–203.
41 S. Arola, J.-M. Malho, P. Laaksonen, M. Lille and M. B. Linder, The role of hemicellulose in nanofibrillated cellulose networks, *Soft Matter*, 2013, **9**, 1319–1326.
42 N. Behabtu, *et al.*, Strong, light, multifunctional fibers of carbon nanotubes with ultrahigh conductivity, *Science*, 2013, **339**, 182–186.
43 E. Frank, F. Hermanutz and M. R. Buchmeiser, Carbon fibers: precursors, manufacturing, and properties, *Macromol. Mater. Eng.*, 2012, **297**, 493–501.
44 M. Nar, *et al.*, Superior plant based carbon fibers from electrospun poly-(caffeyl alcohol) lignin, *Carbon*, 2016, **103**, 372–383.
45 J. H. Grabber, R. D. Hatfield, F. Lu and J. Ralph, Coniferyl ferulate incorporation into lignin enhances the alkaline delignification and enzymatic degradation of cell walls, *Biomacromolecules*, 2008, **9**, 2510–2516.
46 C. G. Wilkerson, *et al.*, Monolignol ferulate transferase introduces chemically labile linkages into the lignin backbone, *Science*, 2014, **344**, 90–93.
47 Q. Li, *et al.*, Discovering biomass structural determinants defining the properties of plant-derived renewable carbon fiber, *iScience*, 2020, **23**, 101405.
48 A. T. Bosch, P. Maissa and P. Sixou, Effect of the flexibility on the phase transition of polymeric liquid crystals, *Phys. Lett. A*, 1983, **94**, 298–300.
49 S. Kubo and J. F. Kadla, Poly(ethylene oxide)/organosolv lignin blends: Relationship between thermal properties, chemical structure, and blend behavior, *Macromolecules*, 2004, **37**, 6904–6911.
50 Y. Uraki, *et al.*, Thermal mobility of *β-O*-4-type artificial lignin, *Biomacromolecules*, 2012, **13**, 867–872.
51 E. Aymerick, *et al.*, Biosynthesis and incorporation of side–chain–truncated lignin monomers to reduce lignin polymerization and enhance saccharification, *Plant Biotechnol. J.*, 2012, **10**, 609–620.
52 V. Ruben, *et al.*, Metabolic engineering of novel lignin in biomass crops, *New Phytol.*, 2012, **196**, 978–1000.